Clim. Past, 18, 1815–1829, 2022
https://doi.org/10.5194/cp-18-1815-2022

Climate of the Past
Open Access
EGU

Compilation of Southern Ocean sea-ice records covering the last glacial-interglacial cycle (12–130 ka)

Matthew Chadwick[1], **Xavier Crosta**[2], **Oliver Esper**[3], **Lena Thöle**[4], **and Karen E. Kohfeld**[5,6]

[1]British Antarctic Survey, Cambridge, UK
[2]UMR 5805 EPOC, Université de Bordeaux, CNRS, EPHE, Pessac, France
[3]Alfred Wegner Institute, Helmholtz Centre for Polar and Marine Research, Bremerhaven, Germany
[4]Department of Earth Sciences, Utrecht University, Utrecht, the Netherlands
[5]School of Resource and Environmental Management, Simon Fraser University, Vancouver, Canada
[6]School of Environmental Science, Simon Fraser University, Vancouver, Canada

Correspondence: Matthew Chadwick (m.chadwick@cornwall-insight.com)

Received: 16 February 2022 – Discussion started: 22 February 2022
Revised: 28 June 2022 – Accepted: 7 July 2022 – Published: 10 August 2022

Abstract. Antarctic sea ice forms a critical part of the Southern Ocean and global climate system. The behaviour of Antarctic sea ice throughout the last glacial-interglacial (G-IG) cycle (12 000–130 000 years) allows us to investigate the interactions between sea ice and climate under a large range of mean climate states. Understanding both temporal and spatial variations in Antarctic sea ice across a G-IG cycle is crucial to a better understanding of the G-IG regulation of atmospheric CO_2, ocean circulation, nutrient cycling and productivity. This study presents 28 published qualitative and quantitative estimates of G-IG sea ice from 24 marine sediment cores and an Antarctic ice core. Sea ice is reconstructed from the sediment core records using diatom assemblages and from the ice core record using sea-salt sodium flux. Whilst all regions of the Southern Ocean display the same overall pattern in G-IG sea-ice variations, the magnitudes and timings vary between regions. Sea-ice cover is most sensitive to changing climate in the regions of high sea-ice outflow from the Weddell Sea and Ross Sea gyres, as indicated by the greatest magnitude changes in sea ice in these areas. In contrast the Scotia Sea sea-ice cover is much more resilient to moderate climatic warming, likely due to the meltwater stratification from high iceberg flux through "iceberg alley" helping to sustain high sea-ice cover outside of full glacial intervals. The differing sensitivities of sea ice to climatic shifts between different regions of the Southern Ocean has important implications for the spatial pattern of nutrient supply and primary productivity, which subsequently impact carbon uptake and atmospheric CO_2 concentrations changes across a G-IG cycle.

1 Introduction

Antarctic sea ice is a crucial component of the Southern Hemisphere and global climate system, through a strong albedo feedback (Hall, 2004), its influence on ocean-atmosphere gas exchange (Rysgaard et al., 2011), its roles in deep and bottom water formation (Rintoul, 2018) and consequently oceanographic circulation (Maksym, 2019). Sea ice helps to stabilise Antarctic ice shelves and marine terminating ice streams by buffering against wave and ocean swell induced calving (Massom et al., 2018). Sea ice is also a crucial habitat for many Antarctic organisms (Arrigo, 2014). Over the last four decades Antarctic sea-ice extent has shown a slight increasing trend, although within the last 5 years there have been 2 years with the lowest annual sea-ice extent in the observational records (Parkinson, 2019). The causes and drivers of this observed sea-ice extent trend are not well understood, with numerous potential mechanisms invoked (Bintanja et al., 2013; Ferreira et al., 2015; Lecomte et al., 2017; Turner et al., 2016). Model simulations struggle with the stochastic nature of the sea-ice system and have been unable to replicate sea-ice changes during the observational period without an unrealistically reduced warming trend (Rosenblum and Eisenman, 2017). In order to better

understand sea-ice changes and diagnose the response of the ocean system to these changes at the multidecadal time scale we must investigate the regional patterns, magnitudes and timing of Antarctic sea-ice changes throughout a full glacial-interglacial (G-IG) cycle. Investigating the last G-IG cycle will allow us to document the interactions between sea ice and climate during both very different mean climate states, such as the warmer than present last Interglacial, and transient climate states, such as glacial terminations or inceptions.

Sea ice has been linked to changes in carbon sequestration, ocean circulation and productivity across G-IG cycles (Kohfeld et al., 2022). Over the last G-IG cycle (12–130 ka) atmospheric CO_2 has been observed to decrease in a stepwise fashion, with at least 3 major intervals of CO_2 drawdown at 115 000–100 000 years (115–100 ka), 72–65 and 40–18 ka (Jouzel et al., 2007). These intervals correspond to the Marine Isotope Stage (MIS) or substage boundaries (MIS 5e-5d, MIS 5a-4 and MIS 3-2, respectively). These changes in atmospheric CO_2 have been tied to several mechanisms operating in the Southern Ocean, including (a) reductions in air-sea gas exchange, (b) enhanced stratification of surface waters, (c) reduced upwelling and vertical diffusion, (d) deep ocean circulation changes and (e) changes in marine biological productivity and nutrient cycling. None of these mechanisms are mutually exclusive, and all can be linked in some way to changes to Antarctic sea-ice cover. Specifically, sea ice regulates deep ocean outgassing through both surface stratification and by acting as a physical barrier (Rysgaard et al., 2011). Brine rejection during sea-ice formation densifies Antarctic bottom waters, thus increasing water column stratification and reducing vertical mixing (Bouttes et al., 2010; Ferrari et al., 2014; Galbraith and de Lavergne, 2019). Both surface and deep stratification of the water column enhance CO_2 sequestration in Southern Ocean abyssal waters. Finally, sea-ice cover in the Southern Ocean influences marine primary productivity, and thus CO_2 uptake, both by acting as a barrier to light and through the release of nutrients, especially iron, in meltwaters within the marginal ice zone (Arrigo et al., 2008). Changes in Southern Ocean sea-ice extent across a G-IG cycle have therefore the potential to play a key role in atmospheric CO_2 variability (Kohfeld and Chase, 2017; Peacock et al., 2006). As a result, understanding the timing and magnitude of sea-ice changes in the Southern Ocean is a crucial question for understanding the G-IG regulation of ocean circulation, productivity, nutrient cycling, and carbon uptake.

Diatom assemblages preserved in marine sediments currently provide the most robust proxy for investigating past changes in Antarctic sea ice over long time intervals (Crosta et al., 2022; Thomas et al., 2019). Sea ice can be reconstructed from past diatom assemblages both qualitatively, using the relative abundance of sea-ice-related diatoms, and quantitatively, using statistical transfer functions. In this study we have compiled both qualitative and quantitative published sea-ice proxy records from 24 Southern Ocean marine sediment cores, alongside 1 Antarctic ice core sea-ice proxy record (Fig. 1), for the last 150 ka, with particular focus on the 12–130 ka interval, to answer the following questions:

- Did different regions of the Southern Ocean display the same patterns of sea-ice advance and retreat across the last G-IG cycle?
- Was the timing and magnitude of sea-ice changes during the last G-IG cycle consistent between different Southern Ocean regions?
- Was sea ice more resilient/sensitive to climatic shifts in the different regions of the Southern Ocean?

2 Materials and methods

2.1 Core sites

We have compiled 28 sea-ice proxy records, whereby 27 records were reconstructed from 24 marine sediment cores (some cores have multiple sea-ice reconstructions utilising different approaches). One record comes from the EPICA Dome C (EDC) ice core (Table 1). Data are presented for the 0–150 ka age range (Fig. 1) but the focus of this study is the 12–130 ka range, as this interval covers a single G-IG cycle from the midpoint of Termination II to the midpoint of Termination I. The data from 0–12 and 130–150 ka are included to give additional insights into Southern Ocean sea-ice behaviour during other G-IG periods. Of the 27 sea-ice proxy records from marine sediment cores, 14 cover the full 12–130 ka interval and the other 13 only cover part of the interval (Table 1). The cores presented in this study are located between 43 and 62° S (Fig. 1), recovered from an average water depth of 3343 m (with a range from 1652 to 5214 m), and the majority are located in the oceanographic region between the modern winter sea-ice extent (WSIE) and the modern Antarctic Polar Front (APF). Almost all diatom-based sea-ice records covering the last G-IG cycle are restricted to the north of the mean WSIE. Retrieving adequate cores south of the mean WSIE is difficult for two reasons. Firstly, heavy sea-ice cover limits biogenic silica production. Secondly, most of this region overlies abyssal plains with depths greater than 4000 m. As a result of both low production and a long settling time, dissolution of the more lightly silicified diatom species (generally sea-ice-related species) increases (Leventer, 1998), which biases the preserved diatom assemblage to reflect warmer and lower sea-ice conditions (Warnock et al., 2015).

We selected records that stretch back beyond 30 ka, to ensure that they cover more than just MIS 2, and also excluded short-term or "snapshot" reconstructions (e.g. the Last Glacial Maximum synthesis by Gersonde et al., 2005, or the MIS 5e synthesis by Chadwick et al., 2020). Any

Table 1. Details for the 24 sediment cores and 1 Antarctic ice core which have sea-ice proxy records presented in this study, including location, temporal coverage and sample resolution of the data, what form the reconstructed sea-ice data comes in and references for both the data and chronology for each record. Cores are ordered by latitude from north to south. FCC: combined relative abundance of the diatom species *Fragilariopsis curta* and *F. cylindrus*, MS: magnetic susceptibility, Na_{ss}: sea-salt sodium, SID: sea-ice duration, SST: sea-surface temperature, WSIC: winter sea-ice concentration.

	Latitude (° S)	Longitude (° E)	Temporal coverage	Sample resolution (ka): mean (min–max)	Sea-ice reconstruction type	Data references	Chronology
SK200/22a	43.70	45.07	2–95	0.8 (0.1–2.1)	SID	Nair et al. (2019)	Radiocarbon ages combined with correlation of the planktonic and benthic δ^{18}O to Antarctic ice cores (Byrd & EDML) and the LR04 δ^{18}O stack (Manoj and Thamban, 2015).
PS2499-5	46.51	−15.33	0–130	1.4 (0.1–4.1)	FCC	Gersonde and Zielinski (2000)	Radiocarbon ages and ^{230}Th excess dating combined with biofluctuation stratigraphies for *Eucampia antarctica* and *Cycladophora davisiana* and planktonic δ^{18}O compared to SPECMAP (Gersonde and Zielinski, 2000).
SK200/27	49.00	45.22	1–73	0.3 (0.1–1.3)	SID	Nair et al. (2019)	Radiocarbon ages combined with correlation of the planktonic and benthic δ^{18}O to Antarctic ice cores (Byrd & EDML) and the LR04 δ^{18}O stack (Manoj and Thamban, 2015).
PS1778-5	49.01	−12.70	12–134	2.3 (0.3–14)	FCC	Gersonde and Zielinski (2000)	Radiocarbon ages and ^{230}Th excess dating combined with biofluctuation stratigraphies for *Eucampia antarctica* and *Cycladophora davisiana* and planktonic δ^{18}O compared to SPECMAP (Gersonde and Zielinski, 2000).
ODP 1093	49.98	5.87	11–150	2.7 (1.1–6.3)	FCC	Schneider Mor et al. (2012)	Correlation of transfer function summer SSTs, *Neogloboquadrina pachyderma* δ^{18}O and MS to δD and dust records from the EDC ice core (Schneider Mor et al., 2012).
PS1768-8	52.59	4.48	3–146	1.6 (0.4–2.6)	WSIC	Esper and Gersonde (2014)	Radiocarbon ages and regional correlation of diatom species composition, estimated summer SSTs and MS between proximal cores (Xiao et al., 2016a) combined with ^{230}Th excess dating (Frank et al., 1996).
PS2102-2	53.07	−4.99	0–35 72–133	1 (0.3–4)	WSIC FCC	Xiao et al. (2016a) Bianchi and Gersonde (2002)	Radiocarbon ages combined with regional correlation of diatom species composition, estimated summer SSTs and MS between proximal cores (Xiao et al., 2016a). *N. pachyderma* δ^{18}O changes compared to SPECMAP combined with diatom biofluctuation zones (Bianchi and Gersonde, 2002).
ODP 1094	53.18	5.13	0–150	2.4 (0.3–4.8)	FCC	Schneider Mor et al. (2012)	Correlation of transfer function summer SSTs, *N. pachyderma* δ^{18}O and MS to δD and dust records from the EDC ice core (Schneider Mor et al., 2012).
TN057-13-PC4	53.20	5.10	0–46	0.9 (0.5–1.9)	SID	Stuut et al. (2004)	Radiocarbon ages (Shemesh et al., 2002).

Table 1. Continued.

	Latitude (° S)	Longitude (° E)	Temporal coverage	Sample resolution (ka): mean (min–max)	Sea-ice reconstruction type	Data references	Chronology
PS2606-6	53.23	40.80	1–36	0.4 (0.1–0.8)	WSIC	Xiao et al. (2016a)	Radiocarbon ages combined with regional correlation of diatom species composition, estimated summer SSTs and MS between proximal cores (Xiao et al., 2016a).
PS1652-2	53.66	5.10	1–33	1.8 (0.7–3.7)	WSIC	Xiao et al. (2016a)	Radiocarbon ages combined with regional correlation of diatom species composition, estimated summer SSTs and MS between proximal cores (Xiao et al., 2016a).
TPC063	53.92	−48.04	0–46	0.4 (0.1–4)	FCC	Collins et al. (2013)	Correlation of relative paleointensity to the SAPIS RPI stack combined with *Eucampia antarctica* biofluctuation stratigraphy (Collins et al., 2012).
PS2276-4	54.64	−23.57	0–130	1.8 (0.5–3.5)	FCC	Gersonde and Zielinski (2000)	Radiocarbon ages and ^{230}Th excess dating combined with biofluctuation stratigraphies for *Eucampia antarctica* and *Cycladophora davisiana* and planktonic δ^{18}O compared to SPECMAP (Gersonde and Zielinski, 2000).
SK200/33	55.02	45.15	6–150	1.5 (0.1–5)	WSIC & SID	Ghadi et al. (2020)	Radiocarbon ages combined with the correlation of SST and SID to the temperature record from the EDC ice core (Ghadi et al., 2020).
PS67/197-1	55.14	−44.11	4–30 30–86	0.4 (0.2–0.7)	WSIC FCC	Xiao et al. (2016a) Xiao (2011)	Radiocarbon ages and regional correlation of Scotia Sea ash layers combined with MS correlation to the EDML ice core dust record, diatom abundance fluctuation patterns and recorded geomagnetic excursions (Xiao et al., 2016b).
TPC078	55.55	−45.02	1–31	1.4 (0.7–2.5)	FCC	Collins et al. (2013)	Radiocarbon ages combined with MS correlation to EDC ice core dust (Collins et al., 2012).
SO136-111	56.67	160.23	3–150	1.1 (0.6–2.2)	SID	Crosta et al. (2004)	Radiocarbon ages combined with the correlation of *N. pachyderma* δ^{18}O to the SPECMAP reference stack (Crosta et al., 2004).
PS67/219-1	57.22	−42.47	5–30 30–150	1 (0.2–10.1)	WSIC FCC	Xiao et al. (2016a) Xiao (2011)	Radiocarbon ages and regional correlation of Scotia Sea ash layers combined with MS correlation to the EDML ice core dust record, diatom abundance fluctuation patterns, recorded geomagnetic excursions and the last common occurrence of *Rouxia leventerae* (Xiao et al., 2016b).
PS75/072-4	57.56	−151.22	1–150	1.1 (0.4–13.7)	FCC	Studer et al. (2015)	Radiocarbon ages and the correlation of δ^{18}O to the LR04 stack combined with regional correlation of elemental composition and MS between proximal cores (Benz et al., 2016).

Table 1. Continued.

	Latitude (° S)	Longitude (° E)	Temporal coverage	Sample resolution (ka): mean (min–max)	Sea-ice reconstruction type	Data references	Chronology
TAN1302-96	59.09	157.05	2–140	1.8 (0.4–6.5)	WSIC & SID	Jones et al. (2022)	Radiocarbon ages combined with the correlation of *N. pachyderma* δ^{18}O to the LR04 stack (Jones et al., 2022).
ELT27-23	59.62	155.24	2–52	1 (0.1–4.9)	WSIC	Ferry et al. (2015a)	Radiocarbon ages combined with the correlation of *N. pachyderma* δ^{18}O to the LR04 stack (Ferry et al., 2015a).
TPC034	59.79	−39.60	0–62	1.8 (0.7–3.3)	FCC	Allen et al. (2011)	*Eucampia antarctica* and *Cycladophora Davisiana* biofluctuation stratigraphies combined with correlation of the MS to EDC ice core dust (Allen et al., 2011).
PS58/271-1	61.24	−116.05	6–148	0.6 (0.2–1.6)	WSIC	Esper and Gersonde (2014)	Correlation of physical parameters, elemental composition, diatom assemblage composition and derived WSIC and SSTs to the EDC ice core record combined with diatom biostratigraphic data (Esper and Gersonde, 2014).
TPC286	61.79	−40.14	0–95	2 (0.2–21.9)	FCC	Collins et al. (2013)	Correlation of relative paleointensity to the SAPIS RPI stack combined with *Eucampia antarctica* biofluctuation stratigraphy (Collins et al., 2012).
EDC	75.10	123.35	1–150	2 (2–2)	Na_{ss} flux	Wolff et al. (2006)	Glaciological ice flow model constrained by dated volcanic horizons and matching of isotopic variations to other ice core records (Parrenin et al., 2007).

records with a mean sample resolution of > 3 ka were also excluded from this synthesis. To avoid additional chronological uncertainties from converting between multiple different age models (e.g. Capron et al., 2014), the chronologies for all the records in this study are kept as originally published. Therefore, the records presented in this study have a chronological uncertainty of $\sim$ 2–4 ka (Bazin et al., 2013b; Lisiecki and Raymo, 2005; Parrenin et al., 2007; Veres et al., 2013), which is not significant compared to the time scale we focus on.

2.2 Sea-ice reconstructions

In this study, we present both quantitative and qualitative reconstructions of sea ice (Fig. 1). Quantitative reconstructions are either the winter sea-ice concentration (WSIC) or the sea-ice duration (SID), with two cores (SK200/33 and TAN1302-96) that have both a WSIC and SID record. All but one (core ELT27-23) of the quantitative reconstructions use a modern analog technique (MAT) diatom transfer function, with cores PS1768-8, PS2102-2, PS2606-6, PS1652-2, PS67/197-1, PS67/219-1 and PS58/271-1 run using the MAT transfer function detailed in Esper and Gersonde (2014) and cores SK200/22a, SK200/27, TN057-13-PC4, SK200/33, SO136-111 and TAN1302-96 run using the MAT transfer function detailed in Crosta et al. (1998) and their evolutions. Core ELT27-23 uses the generalised additive model transfer function detailed in Ferry et al. (2015b). A comparison of reconstructed sea-ice values using both the MAT and generalised additive model transfer functions shows that both techniques yield robust and broadly similar results (Ferry et al., 2015b) and supports our inclusion in this study of records produced with either technique.

For cores where no quantitative sea-ice reconstructions were available we have used a qualitative reconstruction in the form of the combined relative abundance of the diatom species *Fragilariopsis curta* and *F. cylindrus* (FCC). The FCC proxy is a qualitative indicator of winter sea-ice (WSI) presence, with abundances > 3 % associated with locations south of the mean WSI edge (Gersonde and Zielinski, 2000). The sea-salt sodium (Na_{ss}) flux in the EDC ice core is also a qualitative indicator of WSIE, with a higher Na_{ss} flux associated with a greater WSIE (Wolff et al., 2010).

Alongside the raw sea-ice data, we have also normalised all 28 records (Fig. 2) to allow a comparison of the timing of major changes in sea ice between records. We used the

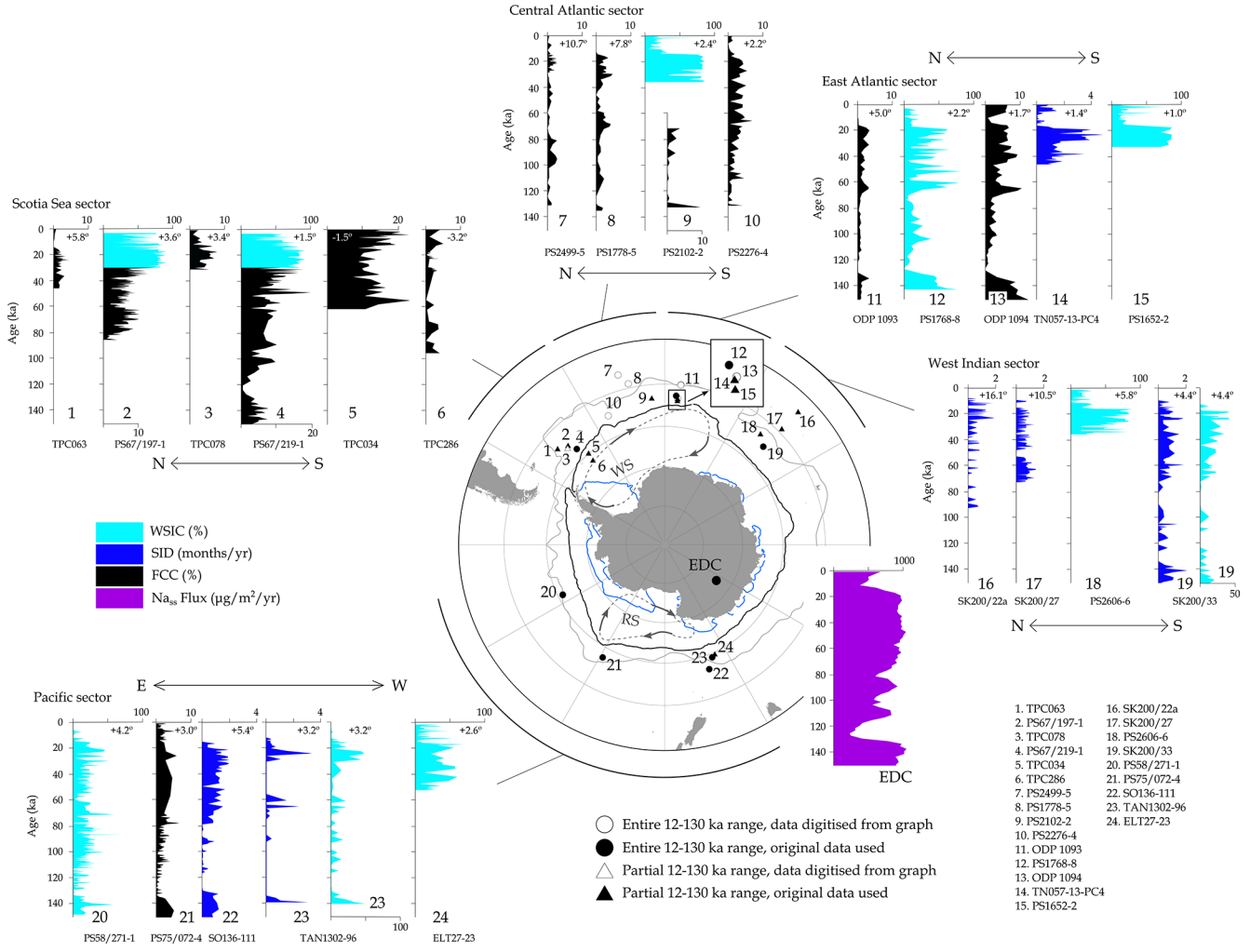

Figure 1. FCC (combined relative abundance of *F. curta* and *F. cylindrus*), WSIC (winter sea-ice concentration) and SID (sea-ice duration) records from Southern Ocean marine sediment cores and the Na_{ss} flux record from the EDC ice core shown alongside a map of Antarctica with core locations, modern February (blue line) and September (black line) sea-ice extents (data from Fetterer et al., 2017) and the modern Antarctic Polar Front position (grey line; Trathan et al., 2000). Dashed lines mark the modern extents of the Weddell Sea (WS) and Ross Sea (RS) gyres. Downcore records are arranged together in Southern Ocean regions, with distance from the modern winter sea-ice (WSI) edge given in degrees latitude (plus sign indicates locations north of the mean WSI edge, minus sign indicates locations south of the mean WSI edge).

following normalisation formula: $(X_{\text{sample}} - X_{\text{mean}})/(X_{\text{max}} - X_{\text{min}})$, where the mean, max and min are calculated using all available data within the 0–150 ka interval for each record. Alongside the individual normalised sea-ice records we also present a stack of normalised records for five different regions of the Southern Ocean (Figs. 2 and 4). In order to stack the normalised records for each region, the individual normalised records were first resampled at 2 ka resolution. This age resolution was chosen as a compromise between maintaining the variation in each record and minimising the amount of interpolation required.

Whilst the normalised records allow us to investigate changes in the timing of major sea-ice changes between records they do not allow a comparison of the magnitude of sea-ice changes. For this comparison we have standardised the quantitative sea-ice records (Fig. 3) using the following formulas: $(X_{\text{WSIC}} - 20)/100$ and $(X_{\text{SID}} - 1)/10$. The 20 % and 1 month yr^{-1} values in the two formulas represent the mean WSIE, north of which sea ice occurs only episodically. This means x-axis values in the Fig. 3 graphs can indicate the relative position of the mean WSI edge, with positive x-axis values indicating periods when the mean WSI edge is located north (equatorward) of the core site and negative values indicating when the mean WSI edge is to the south (poleward) of the core site. The 100 % and 10 months yr^{-1} in the two formulas are scaling factors that show how the WSIC or SID compares to a theoretical maximum. In the modern day, SIDs < 8 months yr^{-1} have a good linear correlation to

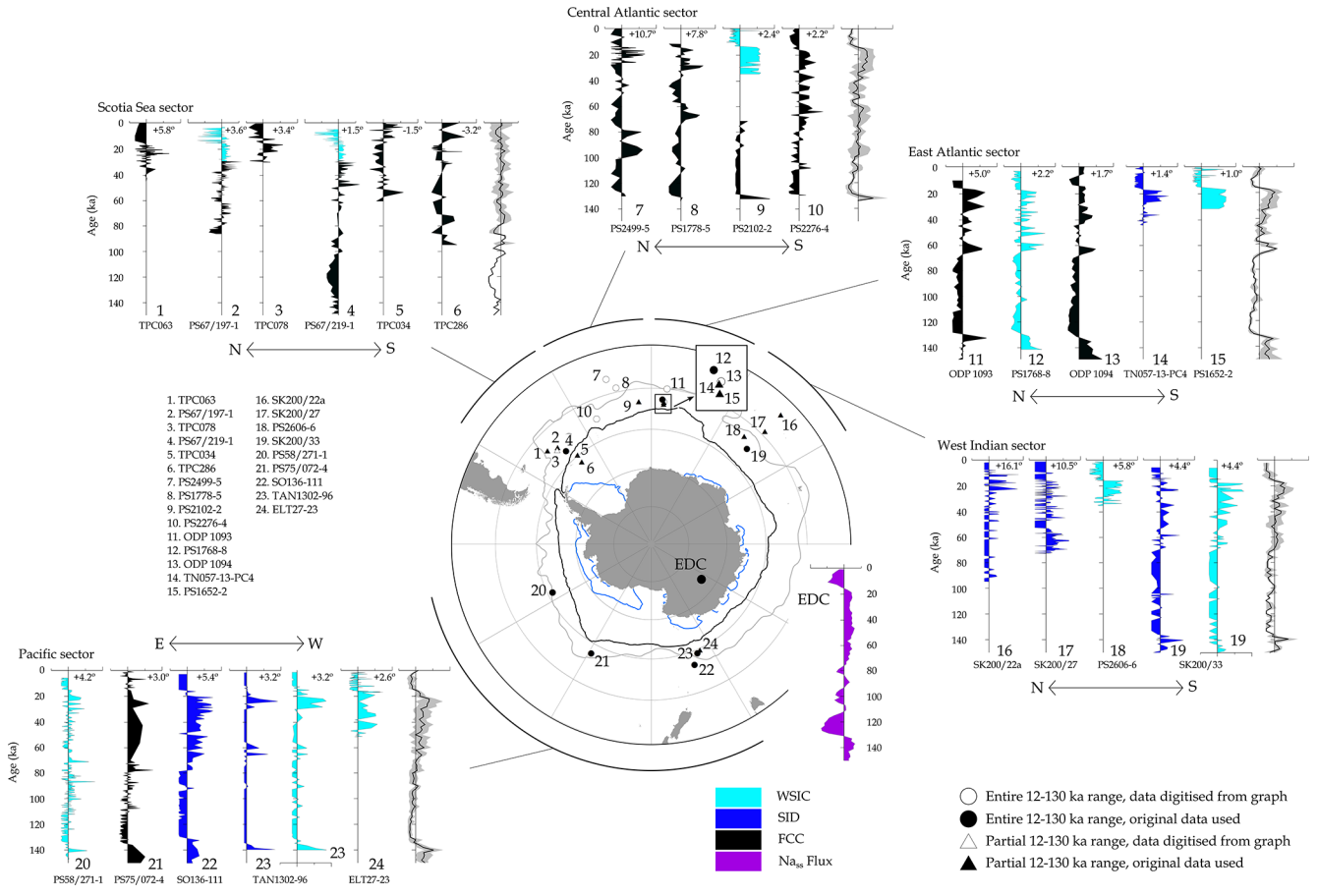

Figure 2. Normalised FCC (combined relative abundance of *F. curta* and *F. cylindrus*), WSIC (winter sea-ice concentration) and SID (sea-ice duration) records from Southern Ocean marine sediment cores and the Na_{ss} flux record from the EDC ice core shown alongside a map of Antarctica with core locations, modern February (blue line) and September (black line) sea-ice extents (data from Fetterer et al., 2017) and the modern Antarctic Polar Front position (grey line; Trathan et al., 2000). Downcore records are arranged together in Southern Ocean regions, with distance from the modern winter sea-ice (WSI) edge given in degrees latitude (plus sign indicates locations north of the mean WSI edge, minus sign indicates locations south of the mean WSI edge). Each region also has a stacked record with the mean (black line) and interquartile range (grey shading) shown.

WSICs (Fig. S1 in the Supplement). Given all the SID values in our records are < 5 months yr^{-1} we have used a theoretical maximum of 10 months yr^{-1} SID to keep this scaling against WSICs, rather than the actual maximum of 12 months yr^{-1} SID. The FCC and Na_{ss} flux proxies are only qualitative indicators of sea ice and cannot be scaled in the same way as the WSIC and SID records. Records with these qualitative proxies are thus excluded from the map of standardised records (Fig. 3).

To allow the comparison of sea-ice patterns and trends between different regions of the Southern Ocean the records in Figs. 1 and 2 are grouped into: the Scotia Sea (60–30° W), the Central Atlantic (30–0° W), the East Atlantic (0–30° E), the West Indian (30–60° E) and the Pacific (150° E–105° W) sectors. These sectors were chosen to allow us to investigate longitudinal variations in sea ice, whilst ensuring there are at least four core records in each sector. In Fig. 3 the Central and East Atlantic sectors are combined into a single Atlantic sector (20° W–30° E) due to the smaller number of standardised records.

2.3 Principal component analysis

A principal component analysis (PCA) was applied to the resampled and normalised data using PAST v3.15 software (Hammer et al., 2001) in order to identify the main trends present in the 27 marine-based sea-ice records (from 24 sites) and the EDC Na_{ss} flux record. We applied the PCA to the normalised data to avoid over-representation of a given proxy or record (e.g. FCC varies between 0 % and 20 % in our records whereas Na_{ss} flux varies between 200 and 1000 µg m^{-2} yr^{-1}). The PCA was performed over the entire 0–150 ka period. Many of the records do not cover the whole

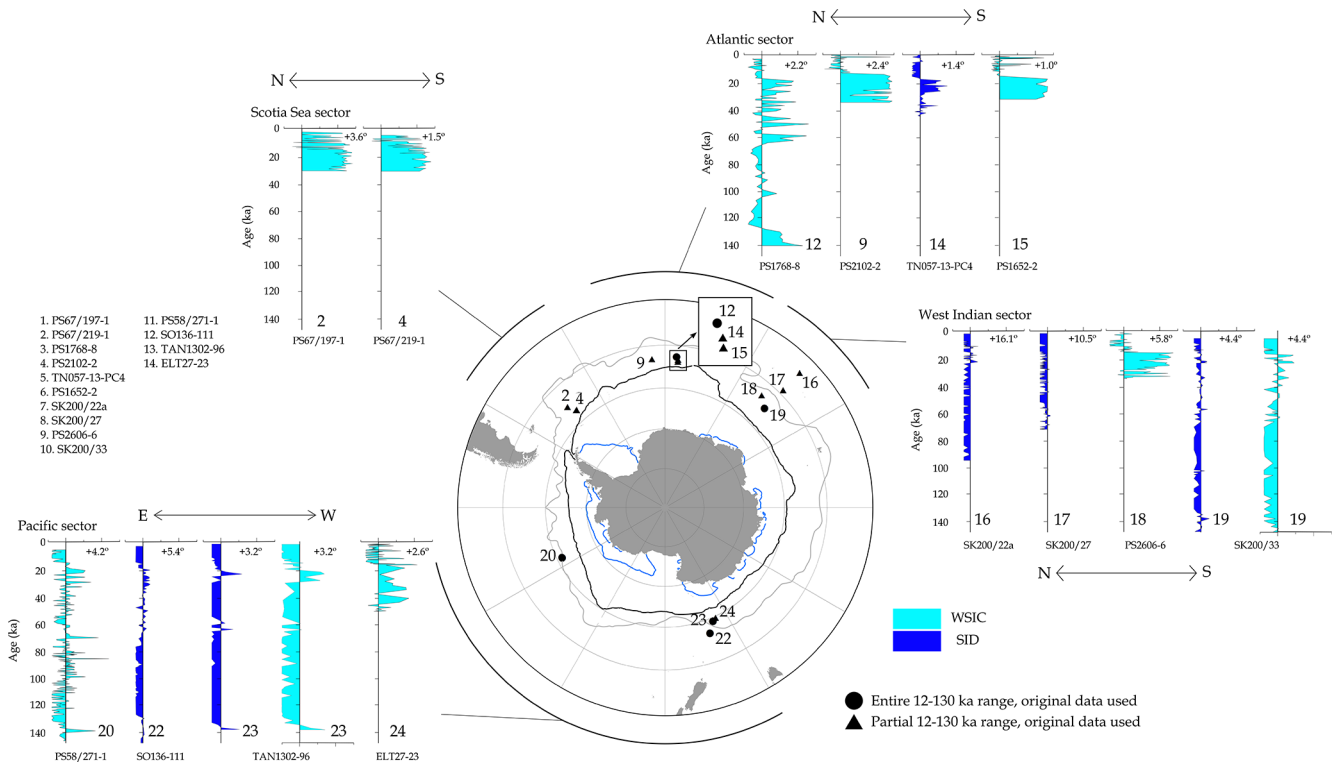

Figure 3. Standardised WSIC (winter sea-ice concentration) and SID (sea-ice duration) records from Southern Ocean marine sediment cores shown alongside a map of Antarctica with core locations, modern February (blue line) and September (black line) sea-ice extents (data from Fetterer et al., 2017) and the modern Antarctic Polar Front position (grey line; Trathan et al., 2000). Downcore records are arranged together in Southern Ocean regions, with distance from the modern winter sea-ice (WSI) edge given in degrees latitude (plus sign indicates locations north of the mean WSI edge, minus sign indicates locations south of the mean WSI edge). Unlike in Figs. 1 and 2, records from the East and Central Atlantic sectors have been combined into a single Atlantic sector region.

period (Fig. 1) and missing values were coped with by using the mean value imputation option.

3 Results and discussion

3.1 Patterns and trends in sea ice

The PCA of all the Southern Ocean sea-ice records in this study reveals that the dominant trend, principal component (PC) 1, in sea ice during the last 130 ka is the G-IG cyclicity, with high sea-ice cover during MIS 2 and low sea ice during MIS 5 (Figs. 4 and S2). PC1 explains 40 % of the total variance, while PC2 accounts for only ∼ 10 % (Fig. S3) and if the PCA is applied solely to the long records, which cover over half of the 0–150 ka interval, PC1 accounts for > 50 % of the variance and PC2 is reduced to 8 %. All PCs except PC1 fall at or below the broken stick curve (Frontier, 1976; Fig. S3) and therefore, only PC1 appears to bear enough signal to be interpreted. The G-IG trend in PC1 is also evident in the normalised stacks for the different sectors of the Southern Ocean, with the exception of the Scotia Sea sector where there is high sea ice throughout the 0–100 ka period (Figs. 2 and 4). The PCA does not produce any grouping based on the different methods of sea-ice reconstruction used (i.e. FCC, WSIC, SID) (Fig. S4), which suggests that all three estimates of sea ice display similar patterns and support our decision to include all three in this study. There is also no apparent PCA grouping by Southern Ocean sector, although the two most southerly Scotia Sea sector cores (TPC034 and TPC286) do have a very different trend to all the other records (Fig. S4).

All Southern Ocean sectors in this study have the same pattern in sea-ice retreat, with a prominent drop during the glacial termination at 140–130 ka, but the pattern in sea-ice advance varies between the sectors (Figs. 1, 2 and 4). The West Indian and Pacific sectors have low sea ice from the glacial termination through until ∼ 80–70 ka, after which the normalised sea-ice values display a gradual increase to maxima at 25–20 ka (Figs. 2 and 4). The East Atlantic sector also has low sea ice until ∼ 70 ka but this is followed by a rapid increase to high normalised sea-ice values during MIS 4 and then a retreat at the beginning of MIS 3, although not as pronounced as during MIS 5 (Fig. 4). Normalised sea-ice values in the East Atlantic then increase gradually from ∼ 55 ka until a maximum concurrent with the other Southern Ocean sectors (Fig. 4). Both the Central Atlantic and Scotia Sea sectors have sea-ice expansion to glacial or near-glacial levels in

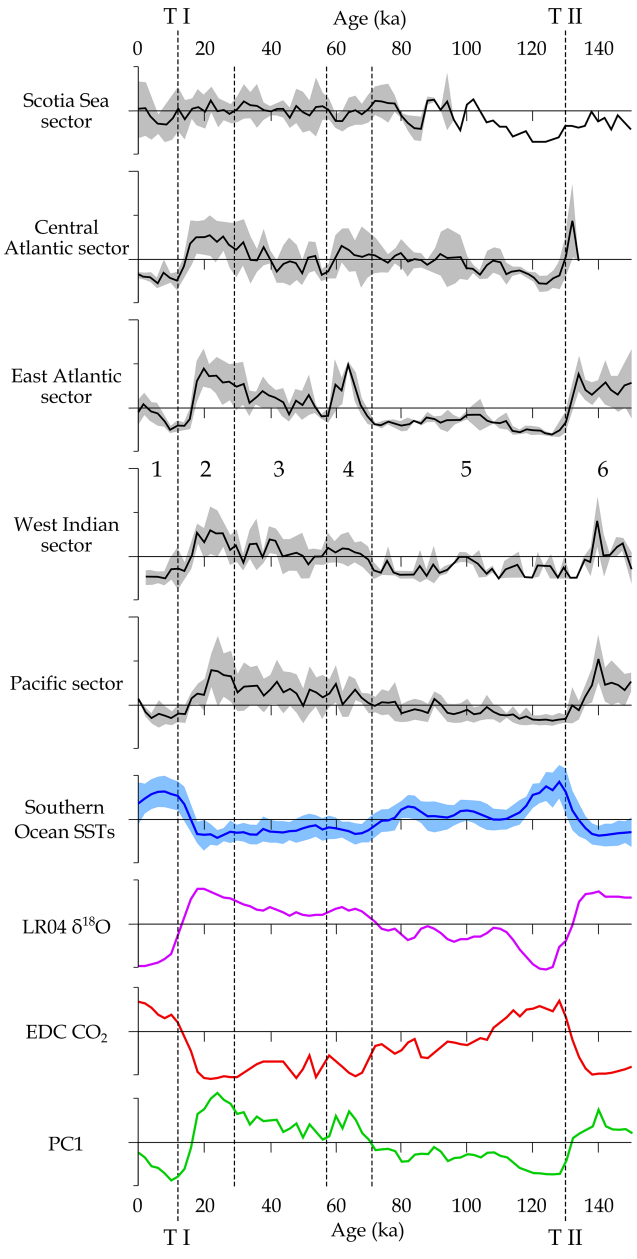

Figure 4. Comparison of the stacks of normalised sea-ice records from the five Southern Ocean sectors (black curves mark the means and grey shading marks the interquartile ranges) alongside the stack of normalised Southern Ocean sea-surface temperature (SST) records (the blue curve marks the mean and the blue shading marks the interquartile range), the normalised LR04 benthic $\delta^{18}O$ stack (purple curve; Lisiecki and Raymo, 2005), the normalised atmospheric CO_2 record from the EDC ice core (red curve; Bazin et al., 2013a) and PC1 (green curve). The selection of the SST data is detailed in Sect. S1. Vertical dashed lines mark MIS boundaries, with each MIS numbered in the centre of the figure.

the normalised values by 100 ka. Normalised sea-ice values in the East Atlantic reach a maximum during the 30–20 ka period in phase with other sectors, except in the Scotia Sea where normalised sea-ice values do not present much variation over the last 100 ka. As such, the pattern in the Central Atlantic sector sea ice indicates a transition between the normalised sea-ice trends in the East Atlantic and Scotia Sea sectors (Figs. 2 and 4). The EDC Na_{ss} flux record has an almost bimodal pattern in values, with both rapid decreases and increases between the interglacial and glacial "states" (Figs. 1 and 2). Between 70 and 20 ka there is almost no variation in the EDC Na_{ss} flux whereas between 130 and 110 ka there is almost a quadrupling of the EDC Na_{ss} flux (Fig. 1). This is in contrast to the trends seen in the sediment core sea-ice records (Figs. 1, 2 and 4) and was suggested by Röthlisberger et al. (2010) to indicate that the Na_{ss} flux in Antarctic ice cores is more sensitive to sea-ice changes during interglacial intervals than during glacial intervals. However, it should be noted that the EPICA Dronning Maud Land (EDML) ice core (75.00° S, 0.07° E) Na_{ss} flux record does show more variation during the 70–20 ka interval (Fischer et al., 2007), which suggests that sea-ice cover may be more dynamic in the Weddell Sea than around the Wilkes Land margin, in agreement with the results in Ghadi et al. (2020).

MIS 5 substages can be seen in both the EDC record and several of the Pacific and Atlantic sector core records (PS1778-5, PS1768-8 and PS75/072-4), whereas the Indian sector records maintain low sea ice from Termination II through until MIS 4 (Fig. 1). The appearance of these substages in the records for cores PS75/072-4 and PS1768-8 (Fig. 1) is likely due to these cores being located near the output regions of the Ross Sea and Weddell Sea gyres, respectively. Both the raw and normalised FCC records from core PS67/219-1 also appear to show MIS 5 substages but with an offset of ∼5 ka to younger ages compared to the other records (Figs. 1 and 2).

For the standardised records in Fig. 3, positive values indicate intervals when the core site is located south of the mean WSI edge. The standardised sea-ice records indicate that the majority of cores with WSIC or SID reconstructions were located within the mean WSIE during MIS 2, with the exception of the most northerly West Indian sector cores (Fig. 3). Our compilation shows that most regions experienced a first significant sea-ice expansion during MIS 4, even though some records indicate that sea ice may have expanded during MIS 5 stadial periods (Figs. 1, 2 and 4). However, a robust assessment of the position of the mean WSI edge prior to MIS 4 is complicated by the scarcity of standardised records for this period (Fig. 3). In the West Indian sector the mean WSI edge was located south of all the core sites in this study until MIS 2 (Fig. 3). In the Pacific sector the SO136-111 and TAN1302-96 core sites were located north of the mean WSI edge during the 130–70 ka interval (MIS 5), with the standardised record for TAN1302-96 indicating it was north of the mean WSI edge during the 130–

25 ka interval (MIS 5 through MIS 3, inclusive). In contrast, the standardised sea-ice record for core PS58/271-1 shows high frequency, but low amplitude, variability around the *y*-axis for the majority of the interval from 110 to 30 ka (Fig. 3), indicating that the mean WSI edge was located at or near this core site throughout this period.

3.2 Magnitude of sea-ice changes

The standardised records show that the largest amplitude changes in sea ice are found in the core records located at the output of the Weddell Sea gyre (Atlantic sector, Fig. 3), indicating that the sea ice in this region is the most sensitive to climate variations. The higher sensitivity of sea ice at the Weddell gyre output than other regions of the Southern Ocean supports the greater sea-ice advance seen in this region in studies of the Last Glacial Maximum (Gersonde et al., 2005) as well as the substantial retreat estimated by model runs of the Last Interglacial (Holloway et al., 2017). The output regions of Southern Ocean gyres are areas of high sea-ice drift in the present day, with changes in Southern Hemisphere winds strongly influencing this drift (Holland and Kwok, 2012; Kwok et al., 2017). As discussed in Sect. 3.1, cores located at the output of the Southern Ocean gyres also show larger normalised sea-ice variations during the colder MIS 5 substages (5b and 5d) than other cores (Fig. 2), further indicating the sensitivity of sea ice in these regions to lower amplitude climatic shifts than full G-IG transitions. Many of the cores in this study, especially those in the West Indian and western Pacific sectors, show relatively little sea-ice signal outside of the higher values during MIS 2-4 (Fig. 1), suggesting that these cores are located too far north to pick up small magnitude changes in sea ice.

In the East and Central Atlantic sectors, the normalised stacks indicate a substantial reduction in sea ice during MIS 3 (Fig. 4). For the Central Atlantic sector stack this trend is largely driven by the normalised sea-ice values in core PS1778-5 (Fig. 2), which is the most easterly Central Atlantic sector core site for which an MIS 3 record is presented (Fig. 2). This behaviour in the two Atlantic sectors contrasts to the normalised stacks for the other Southern Ocean sectors, where high sea ice is maintained throughout the entire MIS 2-4 interval (Fig. 4). In the Pacific sector the only records to show low sea ice during MIS 3 are those from core TAN1302-96, in clear contrast with the nearby SO136-111 and ELT27-23 core records (Fig. 1). However, the lower sea ice during MIS 3 in core TAN1302-96 compared to SO136-111 is attributed to a lower sample resolution in the former (Jones et al., 2022). The reduction in sea ice during MIS 3 in the Central and East Atlantic but not in the other Southern Ocean regions, raises intriguing questions regarding the spatial differences in Antarctic sea-ice sensitivity. Additional records in these other Southern Ocean sectors, at more southerly latitudes, are necessary to assess the robustness of the different sea-ice patterns during MIS 4-3 and the underlying drivers.

The Scotia Sea records indicate an enlarged sea-ice extent, relative to the modern, almost throughout the last 150 ka, with the only exception being during MIS 5e (Fig. 1). The high raw and standardised WSIC values in cores PS67/197-1 and PS67/219-1 indicate that these cores were located south of the mean WSI edge in the Late Holocene at ∼ 4 ka (Figs. 1 and 3). This suggests that the Late Holocene WSI edge in the Scotia Sea was located ∼ 5° further north than its present location. The location of these cores in the modern day "iceberg alley" (Weber et al., 2014) could account for the pervasive sea-ice presence and low sensitivity to climatic variations. A maintained flux of icebergs through this region would release cold and fresh meltwaters, stratifying the surface ocean and promoting sustained sea-ice presence, even during warmer periods. The notable reduction during MIS 5e in the Scotia Sea could therefore either indicate a change in the pathway or flux of Weddell Sea icebergs, or sufficiently warm sea-surface temperatures, maybe as a result of a more southerly position of the Antarctic Circumpolar Current in the Drake Passage and Scotia Sea region (Wu et al., 2021), to outweigh the influence of the iceberg meltwaters. The large amplitude changes in sea ice at the Weddell Sea gyre output, as discussed above, are also likely related to "iceberg alley", with an easterly expansion of the modern iceberg field (Weber et al., 2014) during colder glacial periods providing greater iceberg meltwater stratification in the East Atlantic sector, which promoted and maintained an increased WSIE.

3.3 Timing of sea-ice changes

The different chronologies applied to the records in this study (Table 1) prevent us from being able to identify any small (∼ 2–4 ka) differences in the timing of sea-ice changes between the different Southern Ocean regions. However, during both Termination I and II, we observe up to 5 ka offsets in the retreat time of sea ice between the different regions (Fig. 4). For both the Pacific and West Indian sectors, the normalised stack shows that sea-ice retreat during Termination II started at ∼ 140 ka and was finished by ∼ 130 ka, largely coincident with the increases in both the Southern Ocean SSTs (cores sites shown in Fig. S5) and the atmospheric CO_2 record from the EDC ice core (Figs. 4 and S6). In contrast, the normalised stacks for both the Central and East Atlantic sectors display sea-ice retreat between ∼ 135 and ∼ 125 ka, consistent with the timing of Termination II in the LR04 benthic $\delta^{18}O$ stack (Fig. 4). In the Scotia Sea sector, the only record covering Termination II is from core PS67/219-1 and indicates a longer period of sea-ice retreat lasting from ∼ 140 until ∼ 125 ka (Figs. 1 and 4). The earlier retreat in the West Indian sector compared to the two Atlantic sectors is likely due to the West Indian sector cores being located further north of the modern winter sea-ice extent than the Atlantic sector cores, with an average of 9.2°

of latitude compared to 3.8°, respectively (Fig. 1). However, this does not explain the earlier sea-ice retreat in the Pacific sector, where the cores are located an average of only 3.7° of latitude north of the modern winter sea-ice extent (Fig. 1).

During Termination I, the Pacific sector normalised stack again displays an earlier sea-ice retreat than the other regions, with retreat starting at ∼ 21 ka compared to ∼ 18 ka in the East Atlantic and West Indian sectors and ∼ 16 ka in the Central Atlantic sector (Fig. 4). Whilst the timing of Termination I in the East Atlantic and West Indian sectors occurs within chronological uncertainty of Termination I in either the Central Atlantic or the Pacific sector, these latter regions differ by > 4 ka in their timing for Termination I. The onset of Termination I sea-ice retreat in the East Atlantic, Central Atlantic and West Indian sectors is concurrent with the onset of Southern Hemisphere surface air temperature increases, which dominantly begin at ∼ 17 ka (Osman et al., 2021), and increase in Southern Ocean SSTs (Fig. 4). The earlier sea-ice retreat during Termination I in the East Atlantic sector normalised stack, compared to the Central Atlantic sector stack, is likely due to the proximity of the eastern core sites to the Weddell Sea gyre output. Gersonde et al. (2005) reconstructed a "tongue" of summer sea ice in this region during the Last Glacial Maximum which suggests sea ice in this area is more dynamic and may have been more susceptible to early melting and retreat during Termination I than the sea ice located further west. The discrepancy between the earlier retreat of sea ice in the East Atlantic sector, relative to the Central Atlantic sector, during Termination I but not Termination II could indicate that either the sea-ice "tongue" in the East Atlantic sector was more resilient to melting and retreat during MIS 6 than during MIS 2, or that this "tongue" did not exist during MIS 6. The high sensitivity of East Atlantic sector sea ice during Termination I is also indicated by the rapid retreat to interglacial levels, with a deglaciation duration of only ∼ 2–4 ka compared to the ∼ 5–8 ka deglaciation duration in the other Southern Ocean sectors (Fig. 4). The normalised stack for the Scotia Sea does not show any clear signal for Termination I (Fig. 4), with only cores TPC063 and TPC078 displaying the sharp decrease in sea ice between 20 and 12 ka that characterises Termination I in the other records (Fig. 1).

4 Summary and outstanding questions

The present compilation of sea-ice records suggests that all regions of the Southern Ocean display the same general pattern in sea ice during the last G-IG cycle, with high sea ice during MIS 2 and 4 and low sea ice during MIS 5e. However, the different areas of the Southern Ocean do have varying magnitudes, timing and short-term trends in sea ice during the 12–130 ka interval, especially with respect to sea-ice advance between MIS 5e and 4. Sea-ice cover seems to be most sensitive to changing climate at the outputs of the Weddell Sea and Ross Sea gyres, with the greatest magnitude sea-ice changes occurring in cores located in these regions. Records located near the Weddell Sea gyre output have especially high sensitivity, with a more rapid sea-ice advance and retreat than other areas of the Southern Ocean and a more pronounced MIS 3 sea-ice reduction than the other regions. In contrast, the sea-ice cover in the Scotia Sea region is seemingly much more resilient to changing climate, with the only notable reduction during the peak of the MIS 5e interglacial. This resilience to moderate warming could be related to the large iceberg flux through the Scotia Sea, with iceberg-meltwater stratification and cooling helping to sustain sea ice outside of full glacial intervals.

By compiling long-term sea-ice records of the last G-IG cycle from throughout the Southern Ocean this study has identified how changes in sea ice vary between different regions of the Southern Ocean. The more dynamic state of sea ice in the East Atlantic over long time scales is likely associated with the expansion and contraction of "iceberg alley". Weddell Sea icebergs have been identified as an important source of iron to the Atlantic sector of the Southern Ocean (Shaw et al., 2011) and large amplitude changes in the spatial extent of iceberg outflow over G-IG cycles therefore helps explain the high magnitude variations in G-IG iron flux in this region of the Southern Ocean (Martínez-Garcia et al., 2009). Large amplitude changes in both the East Atlantic sector WSIE and the spatial extent of "iceberg alley" over a G-IG cycle have important implications for the supply of nutrients, especially iron, and subsequently primary productivity in this region. This, in turn, helps regulate oceanic CO_2 sequestration across a G-IG cycle, in an area of the Southern Ocean with high modern primary productivity (Vernet et al., 2019).

Our compilation also allows us to identify where further research would most help to develop the results and findings of this study. It is clear from the discussion in Sect. 3.3 that establishing a harmonised chronology across all core records could help reduce the ∼ 2–4 ka chronological uncertainties presented in this study and allow further analysis of any short duration leads and lags between the sea-ice changes in the different Southern Ocean sectors. Alongside an improved chronology, N-S transects of sea-ice records, especially in the regions with the highest amplitude of G-IG sea-ice variability (e.g. East Atlantic sector), would allow the rates of sea-ice advance and retreat to be estimated. A refined chronology would also allow sea-ice dynamics to be compared between hemispheres and provide insights into how sea ice influences global ocean circulation dynamics across a G-IG cycle.

Model-proxy comparisons of sea-ice extent over the last 130 ka display mixed results, with good agreement between model and proxy estimates of WSIE during the Last Glacial Maximum (Green et al., 2022) but poor model-data consistency in estimates of summer sea-ice extent during the Last Glacial Maximum (Green et al., 2022) and WSIE during the Last Interglacial (Chadwick et al., 2022a; Otto-Bliesner et

al., 2021). Antarctic sea-ice changes during the observational period have also not been replicated in model simulations, without an unrealistically reduced warming trend (Rosenblum and Eisenman, 2017). Better parameterisation of sea ice (and assimilation of proxy records) is required to improve our understanding of the drivers and feedbacks active over both short and long time scales.

Finally, whilst this study presents a good spatial coverage in some areas of the Southern Ocean (e.g. the Atlantic sector), there are parts of the Southern Ocean for which G-IG sea-ice changes are minimally constrained (Figs. 1–3). The central and eastern Pacific sector (90–180° W) currently has only two long G-IG sea-ice records and the eastern Indian sector (60–150° E) has none. Similarly, the majority of the G-IG sea-ice records presented here are located north of the modern mean WSIE (Figs. 1–3), largely due to the difficulties associated with reconstructing robust sea-ice estimates from diatom records located beneath persistent or long duration sea-ice cover (as discussed in Sect. 2.1). The development of new sea-ice proxies from beneath this persistent sea ice, e.g. highly branched isoprenoids (Belt, 2018; Lamping et al., 2021; Vorrath et al., 2019) or DNA from sea-ice associated organisms (De Schepper et al., 2019), could allow the reconstruction of sea ice from more southerly core sites, without which any small amplitude sea-ice variations during warmer interglacial periods (e.g. MIS 5a, 5c and 5e) cannot be fully investigated.

Data availability. The sea-ice proxy data for all 27 marine sediment core records are available from PANGAEA (https://doi.org/10.1594/PANGAEA.943275, Chadwick et al., 2022b).

Supplement. The supplement related to this article is available online at: https://doi.org/10.5194/cp-18-1815-2022-supplement.

Author contributions. MC contributed to the conceptualisation, data curation, formal analysis, investigation, methodology, visualisation and writing the original draft. XC contributed to the conceptualisation, formal analysis, methodology, resources, supervision, visualisation and reviewing and editing the writing. OE contributed to the conceptualisation, resources and reviewing and editing the writing. LT contributed to the data curation, investigation and resources. KEK contributed to the conceptualisation, funding acquisition, investigation, project administration, supervision and reviewing and editing the writing.

Competing interests. The contact author has declared that none of the authors has any competing interests.

Disclaimer. Publisher's note: Copernicus Publications remains neutral with regard to jurisdictional claims in published maps and institutional affiliations.

Special issue statement. This article is part of the special issue "Reconstructing Southern Ocean sea-ice dynamics on glacial to historical time scales". It is not associated with a conference.

Acknowledgements. This work was conducted as part of Phase 1 of the Cycles of Sea-Ice Dynamics in the Earth system (C-SIDE) PAGES scientific working group. We thank both Claire S. Allen and Jacob Jones for directly providing us with their sea-ice proxy records from cores TPC034 and TAN1302-96, respectively.

Financial support. This research has been supported by a Past Global Changes Data Stewardship Scholarship (grant no. DSS_105) for Matthew Chadwick and a National Sciences and Engineering Research Council of Canada Discovery Grant (grant no. RGPIN342251) for Karen E. Kohfeld.

Review statement. This paper was edited by Marit-Solveig Seidenkrantz and reviewed by two anonymous referees.

References

Allen, C. S., Pike, J., and Pudsey, C. J.: Last glacial–interglacial sea-ice cover in the SW Atlantic and its potential role in global deglaciation, Quaternary Sci. Rev., 30, 2446–2458, 2011.

Arrigo, K. R.: Sea ice ecosystems, Annu. Rev. Mar. Sci., 6, 439–467, 2014.

Arrigo, K. R., van Dijken, G. L., and Bushinsky, S.: Primary production in the Southern Ocean, 1997–2006, J. Geophys. Res., 113, C08004, https://doi.org/10.1029/2007JC004551, 2008.

Bazin, L., Landais, A., Lemieux-Dudon, B., Toyé Mahamadou Kele, H., Veres, D., Parrenin, F., Martinerie, P., Ritz, C., Capron, E., Lipenkov, V., Loutre, M. F., Raynaud, D., Vinther, B., Svensson, A., Rasmussen, S. O., Severi, M., Blunier, T., Leuenberger, M., Fischer, H., Masson-Delmotte, V., Chappellaz, J., and Wolff, E.: Carbon dioxide composite data on AICC2012 chronology, PANGAEA, https://doi.org/10.1594/PANGAEA.824893, 2013a.

Bazin, L., Landais, A., Lemieux-Dudon, B., Toyé Mahamadou Kele, H., Veres, D., Parrenin, F., Martinerie, P., Ritz, C., Capron, E., Lipenkov, V., Loutre, M.-F., Raynaud, D., Vinther, B., Svensson, A., Rasmussen, S. O., Severi, M., Blunier, T., Leuenberger, M., Fischer, H., Masson-Delmotte, V., Chappellaz, J., and Wolff, E.: An optimized multi-proxy, multi-site Antarctic ice and gas orbital chronology (AICC2012): 120–800 ka, Clim. Past, 9, 1715–1731, https://doi.org/10.5194/cp-9-1715-2013, 2013b.

Belt, S. T.: Source-specific biomarkers as proxies for Arctic and Antarctic sea ice, Org. Geochem., 125, 277–298, 2018.

Benz, V., Esper, O., Gersonde, R., Lamy, F., and Tiedemann, R.: Last Glacial Maximum sea surface temperature and sea-ice extent in the Pacific sector of the Southern Ocean, Quaternary Sci. Rev., 146, 216–237, 2016.

Bianchi, C. and Gersonde, R.: The Southern Ocean surface between Marine Isotope Stages 6 and 5d: Shape and timing of climate changes, Palaeogeogr. Palaeocl., 187, 151–177, 2002.

Bintanja, R., van Oldenborgh, G. J., Drijfhout, S. S., Wouters, B., and Katsman, C. A.: Important role for ocean warming and increased ice-shelf melt in Antarctic sea-ice expansion, Nat. Geosci., 6, 376–379, 2013.

Bouttes, N., Paillard, D., and Roche, D. M.: Impact of brine-induced stratification on the glacial carbon cycle, Clim. Past, 6, 575–589, https://doi.org/10.5194/cp-6-575-2010, 2010.

Capron, E., Govin, A., Stone, E. J., Masson-Delmotte, V., Mulitza, S., Otto-Bliesner, B., Rasmussen, T. L., Sime, L. C., Waelbroeck, C., and Wolff, E. W.: Temporal and spatial structure of multi-millennial temperature changes at high latitudes during the Last Interglacial, Quaternary Sci. Rev., 103, 116–133, 2014.

Chadwick, M., Allen, C. S., Sime, L. C., and Hillenbrand, C. D.: Analysing the timing of peak warming and minimum winter sea-ice extent in the Southern Ocean during MIS 5e, Quaternary Sci. Rev., 229, 106134, https://doi.org/10.1016/j.quascirev.2019.106134, 2020.

Chadwick, M., Sime, L. C., Allen, C. S., Guarino, M.-V., and Oliver, K. I. C.: Model-data comparison of Antarctic winter sea-ice extent and Southern Ocean sea-surface temperatures during MIS 5e, Earth Planet. Sci. Lett., in review, 2022a.

Chadwick, M., Crosta, X., Esper, O., and Kohfeld, K. E.: Southern Ocean marine sediment core sea-ice records for the last 150 000 years, PANGAEA [data set], https://doi.org/10.1594/PANGAEA.943275, 2022b.

Collins, L. G., Pike, J., Allen, C. S., and Hodgson, D. A.: High-resolution reconstruction of southwest Atlantic sea-ice and its role in the carbon cycle during marine isotope stages 3 and 2, Paleoceanography, 27, PA3217, https://doi.org/10.1029/2011pa002264, 2012.

Collins, L. G., Allen, C. S., Pike, J., Hodgson, D. A., Weckström, K., and Massé, G.: Evaluating highly branched isoprenoid (HBI) biomarkers as a novel Antarctic sea-ice proxy in deep ocean glacial age sediments, Quaternary Sci. Rev., 79, 87–98, 2013.

Crosta, X., Pichon, J. J., and Burckle, L. H.: Application of modern analog technique to marine Antarctic diatoms: Reconstruction of maximum sea-ice extent at the Last Glacial Maximum, Paleoceanography, 13, 284–297, 1998.

Crosta, X., Sturm, A., Armand, L., and Pichon, J.-J.: Late Quaternary sea ice history in the Indian sector of the Southern Ocean as recorded by diatom assemblages, Mar. Micropaleontol., 50, 209–223, 2004.

Crosta, X., Kohfeld, K. E., Bostock, H. C., Chadwick, M., Du Vivier, A., Esper, O., Etourneau, J., Jones, J., Leventer, A., Müller, J., Rhodes, R. H., Allen, C. S., Ghadi, P., Lamping, N., Lange, C., Lawler, K.-A., Lund, D., Marzocchi, A., Meissner, K. J., Menviel, L., Nair, A., Patterson, M., Pike, J., Prebble, J. G., Riesselman, C., Sadatzki, H., Sime, L. C., Shukla, S. K., Thöle, L., Vorrath, M.-E., Xiao, W., and Yang, J.: Antarctic sea ice over the past 130,000 years, Part 1: A review of what proxy records tell us, EGUsphere [preprint], https://doi.org/10.5194/egusphere-2022-99, 2022.

De Schepper, S., Ray, J. L., Skaar, K. S., Sadatzki, H., Ijaz, U. Z., Stein, R., and Larsen, A.: The potential of sedimentary ancient DNA for reconstructing past sea ice evolution, ISME J., 13, 2566–2577, 2019.

Esper, O. and Gersonde, R.: New tools for the reconstruction of Pleistocene Antarctic sea ice, Palaeogeog. Palaeocl., 399, 260–283, 2014.

Ferrari, R., Jansen, M. F., Adkins, J. F., Burke, A., Stewart, A. L., and Thompson, A. F.: Antarctic sea ice control on ocean circulation in present and glacial climates, P. Natl. Acad. Sci. USA, 111, 8753–8758, 2014.

Ferreira, D., Marshall, J., Bitz, C. M., Solomon, S., and Plumb, A.: Antarctic Ocean and Sea Ice Response to Ozone Depletion: A Two-Time-Scale Problem, J. Climate, 28, 1206–1226, 2015.

Ferry, A. J., Crosta, X., Quilty, P. G., Fink, D., Howard, W., and Armand, L. K.: First records of winter sea ice concentration in the southwest Pacific sector of the Southern Ocean, Paleoceanography, 30, 1525–1539, 2015a.

Ferry, A. J., Prvan, T., Jersky, B., Crosta, X., and Armand, L. K.: Statistical modeling of Southern Ocean marine diatom proxy and winter sea ice data: Model comparison and developments, Prog. Oceanogr., 131, 100–112, 2015b.

Fetterer, F., Knowles, K., Meier, W. N., Savoie, M., and Windnagel, A. K.: Sea Ice Index, Version 3. NSIDC: National Snow and Ice Data Center, Boulder, Colorado USA, https://doi.org/10.7265/N5K072F8, 2017.

Fischer, H., Fundel, F., Ruth, U., Twarloh, B., Wegner, A., Udisti, R., Becagli, S., Castellano, E., Morganti, A., Severi, M., Wolff, E., Littot, G., Röthlisberger, R., Mulvaney, R., Hutterli, M. A., Kaufmann, P., Federer, U., Lambert, F., Bigler, M., Hansson, M., Jonsell, U., de Angelis, M., Boutron, C., Siggaard-Andersen, M.-L., Steffensen, J. P., Barbante, C., Gaspari, V., Gabrielli, P., and Wagenbach, D.: Reconstruction of millennial changes in dust emission, transport and regional sea ice coverage using the deep EPICA ice cores from the Atlantic and Indian Ocean sector of Antarctica, Earth Planet. Sc. Lett., 260, 340–354, 2007.

Frank, M., Gersonde, R., Rutgers van der Loeff, M., Kuhn, G., and Mangini, A.: Late Quaternary sediment dating and quantification of lateral sediment redistribution applying 230Thex: a study from the eastern Atlantic sector of the Southern Ocean, Geol. Rundsch., 85, 544–566, 1996.

Frontier, S.: Étude de la décroissance des valeurs propres dans une analyse en composantes principales: comparaison avec le modèle du bâton brisé, J. Exp. Mar. Biol. Ecol., 25, 67–75, 1976.

Galbraith, E. and de Lavergne, C.: Response of a comprehensive climate model to a broad range of external forcings: relevance for deep ocean ventilation and the development of late Cenozoic ice ages, Clim. Dynam., 52, 653–679, 2019.

Gersonde, R. and Zielinski, U.: The reconstruction of late Quaternary Antarctic sea-ice distribution – the use of diatoms as a proxy for sea-ice, Palaeogeogr. Palaeocl., 162, 263–286, 2000.

Gersonde, R., Crosta, X., Abelmann, A., and Armand, L.: Sea-surface temperature and sea ice distribution of the Southern Ocean at the EPILOG Last Glacial Maximum – a circum-Antarctic view based on siliceous microfossil records, Quaternary Sci. Rev., 24, 869–896, 2005.

Ghadi, P., Nair, A., Crosta, X., Mohan, R., Manoj, M. C., and Meloth, T.: Antarctic sea-ice and palaeoproductivity variation over the last 156 000 years in the Indian sector of Southern Ocean, Mar. Micropaleontol., 160, 101894, https://doi.org/10.1016/j.marmicro.2020.101894, 2020.

Green, R. A., Menviel, L., Meissner, K. J., Crosta, X., Chandan, D., Lohmann, G., Peltier, W. R., Shi, X., and Zhu, J.: Evaluating sea-

sonal sea-ice cover over the Southern Ocean at the Last Glacial Maximum, Clim. Past, 18, 845–862, https://doi.org/10.5194/cp-18-845-2022, 2022.

Hall, A.: The Role of Surface Albedo Feedback in Climate, J. Climate, 17, 1550–1568, 2004.

Hammer, O., Harper, D. A. T., and Ryan, P. D.: Past: Paleontological Statistics Software Package for Education and Data Analysis, Palaeontologica Electronica, 4, 9, http://palaeo-electronica.org/2001_1/past/issue1_01.htm (last access: 3 August 2022), 2001.

Holland, P. R. and Kwok, R.: Wind-driven trends in Antarctic sea-ice drift, Nat. Geosci., 5, 872–875, 2012.

Holloway, M. D., Sime, L. C., Allen, C. S., Hillenbrand, C.-D., Bunch, P., Wolff, E., and Valdes, P. J.: The spatial structure of the 128 ka Antarctic sea ice minimum, Geophys. Res. Lett., 44, 11129–11139, 2017.

Jones, J., Kohfeld, K. E., Bostock, H., Crosta, X., Liston, M., Dunbar, G., Chase, Z., Leventer, A., Anderson, H., and Jacobsen, G.: Sea ice changes in the southwest Pacific sector of the Southern Ocean during the last 140 000 years, Clim. Past, 18, 465–483, https://doi.org/10.5194/cp-18-465-2022, 2022.

Jouzel, J., Masson-Delmotte, V., Cattani, O., Dreyfus, G., Falourd, S., Hoffmann, G., Minster, B., Nouet, J., Barnola, J.-M., Chappellaz, J., Fischer, H., Gallet, J. C., Johnsen, S. J., Leuenberger, M., Loulergue, L., Luethi, D., Oerter, H., Parrenin, F., Raisbeck, G., Raynaud, D., Schilt, A., Schwander, J., Selmo, E., Souchez, R., Spahni, R., Stauffer, B., Steffensen, J. P., Stenni, B., Stocker, T. F., Tison, J.-L., Werner, M., and Wolff, E. W.: Orbital and Millennial Antarctic Climate Variability over the Past 800 000 Years, Science, 317, 793–796, 2007.

Kohfeld, K. E. and Chase, Z.: Temporal evolution of mechanisms controlling ocean carbon uptake during the last glacial cycle, Earth Planet. Sci. Lett., 472, 206–215, 2017.

Kohfeld, K. E., Bostock, H. C., Crosta, X., Leventer, A., Meissner, K., Chadwick, M., Lowe, V., Jaccard, S. L., Skinner, L., Chase, Z., Marzocchi, A., Thöle, L., Mix, A., Lund, D., Menviel, L., Sime, L. C., Missiaen, L., Lawler, K.-A., Sikes, E., Eby, M., and Zickfield, K.: Past changes in Antarctic sea ice, Part 2: Implications for ocean circulation, biogeochemical cycling, and global climate, in preparation, 2022.

Kwok, R., Pang, S. S., and Kacimi, S.: Sea ice drift in the Southern Ocean: Regional patterns, variability, and trends, Elem. Sci. Anth., 5, 1–16, 2017.

Lamping, N., Müller, J., Hefter, J., Mollenhauer, G., Haas, C., Shi, X., Vorrath, M.-E., Lohmann, G., and Hillenbrand, C.-D.: Evaluation of lipid biomarkers as proxies for sea ice and ocean temperatures along the Antarctic continental margin, Clim. Past, 17, 2305–2326, https://doi.org/10.5194/cp-17-2305-2021, 2021.

Lecomte, O., Goosse, H., Fichefet, T., de Lavergne, C., Barthelemy, A., and Zunz, V.: Vertical ocean heat redistribution sustaining sea-ice concentration trends in the Ross Sea, Nat. Commun., 8, 258, https://doi.org/10.1038/s41467-017-00347-4, 2017.

Leventer, A.: The fate of Antarctic "sea ice diatoms" and their use as paleoenvironmental indicators, in: Antarctic Sea-ice, Biological Processes, Interactions and Variability, edited by: Lizotte, M. P. and Arrigo, K. R., Antarctic Research Series, American Geophysical Union, Washington D.C., USA, 73, 121–137, https://agupubs.onlinelibrary.wiley.com/doi/epdf/10.1029/AR073p0121?saml_referrer (last access: 8 August 2022), 1998.

Lisiecki, L. E. and Raymo, M. E.: A Pliocene-Pleistocene stack of 57 globally distributed benthic δ^{18}O records, Paleoceanography, 20, PA1003, https://doi.org/10.1029/2004pa001071, 2005.

Maksym, T.: Arctic and Antarctic Sea Ice Change: Contrasts, Commonalities, and Causes, Annu. Rev. Mar. Sci., 11, 187–213, 2019.

Manoj, M. C. and Thamban, M.: Shifting frontal regimes and its influence on bioproductivity variations during the Late Quaternary in the Indian sector of Southern Ocean, Deep-Sea Res. Pt. II, 118, 261–274, 2015.

Martínez-Garcia, A., Rosell-Melé, A., Geibert, W., Gersonde, R., Masqué, P., Gaspari, V., and Barbante, C.: Links between iron supply, marine productivity, sea surface temperature, and CO_2 over the last 1.1 Ma, Paleoceanography, 24, PA1207, https://doi.org/10.1029/2008pa001657, 2009.

Massom, R. A., Scambos, T. A., Bennetts, L. G., Reid, P., Squire, V. A., and Stammerjohn, S. E.: Antarctic ice shelf disintegration triggered by sea ice loss and ocean swell, Nature, 558, 383–389, 2018.

Nair, A., Mohan, R., Crosta, X., Manoj, M. C., Thamban, M., and Marieu, V.: Southern Ocean sea ice and frontal changes during the Late Quaternary and their linkages to Asian summer monsoon, Quaternary Sci. Rev., 213, 93–104, 2019.

Osman, M. B., Tierney, J. E., Zhu, J., Tardif, R., Hakim, G. J., King, J., and Poulsen, C. J.: Globally resolved surface temperatures since the Last Glacial Maximum, Nature, 599, 239–244, 2021.

Otto-Bliesner, B. L., Brady, E. C., Zhao, A., Brierley, C. M., Axford, Y., Capron, E., Govin, A., Hoffman, J. S., Isaacs, E., Kageyama, M., Scussolini, P., Tzedakis, P. C., Williams, C. J. R., Wolff, E., Abe-Ouchi, A., Braconnot, P., Ramos Buarque, S., Cao, J., de Vernal, A., Guarino, M. V., Guo, C., LeGrande, A. N., Lohmann, G., Meissner, K. J., Menviel, L., Morozova, P. A., Nisancioglu, K. H., O'ishi, R., Salas y Mélia, D., Shi, X., Sicard, M., Sime, L., Stepanek, C., Tomas, R., Volodin, E., Yeung, N. K. H., Zhang, Q., Zhang, Z., and Zheng, W.: Large-scale features of Last Interglacial climate: results from evaluating the *lig127k* simulations for the Coupled Model Intercomparison Project (CMIP6)–Paleoclimate Modeling Intercomparison Project (PMIP4), Clim. Past, 17, 63–94, https://doi.org/10.5194/cp-17-63-2021, 2021.

Parkinson, C. L.: A 40-y record reveals gradual Antarctic sea ice increases followed by decreases at rates far exceeding the rates seen in the Arctic, P. Natl. Acad. Sci. USA, 116, 14414–14423, 2019.

Parrenin, F., Barnola, J.-M., Beer, J., Blunier, T., Castellano, E., Chappellaz, J., Dreyfus, G., Fischer, H., Fujita, S., Jouzel, J., Kawamura, K., Lemieux-Dudon, B., Loulergue, L., Masson-Delmotte, V., Narcisi, B., Petit, J.-R., Raisbeck, G., Raynaud, D., Ruth, U., Schwander, J., Severi, M., Spahni, R., Steffensen, J. P., Svensson, A., Udisti, R., Waelbroeck, C., and Wolff, E.: The EDC3 chronology for the EPICA Dome C ice core, Clim. Past, 3, 485–497, https://doi.org/10.5194/cp-3-485-2007, 2007.

Peacock, S., Lane, E., and Restrepo, J. M.: A possible sequence of events for the generalized glacial-interglacial cycle, Global Biogeochem. Cy., 20, GB2010, https://doi.org/10.1029/2005gb002448, 2006.

Rintoul, S. R.: The global influence of localized dynamics in the Southern Ocean, Nature, 558, 209–218, 2018.

Rosenblum, E. and Eisenman, I.: Sea Ice Trends in Climate Models Only Accurate in Runs with Biased Global Warming, J. Climate, 30, 6265–6278, 2017.

Röthlisberger, R., Crosta, X., Abram, N. J., Armand, L., and Wolff, E. W.: Potential and limitations of marine and ice core sea ice proxies: an example from the Indian Ocean sector, Quaternary Sci. Rev., 29, 296–302, 2010.

Rysgaard, S., Bendtsen, J., Delille, B., Dieckmann, G. S., Glud, R. N., Kennedy, H., Mortensen, J., Papadimitriou, S., Thomas, D. N., and Tison, J.-L.: Sea ice contribution to the air–sea CO_2 exchange in the Arctic and Southern Oceans, Tellus B, 63, 823–830, 2011.

Schneider Mor, A., Yam, R., Bianchi, C., Kunz-Pirrung, M., Gersonde, R., and Shemesh, A.: Variable sequence of events during the past seven terminations in two deep-sea cores from the Southern Ocean, Quaternary Res., 77, 317–325, 2012.

Shaw, T. J., Raiswell, R., Hexel, C. R., Vu, H. P., Moore, W. S., Dudgeon, R., and Smith, K. L.: Input, composition, and potential impact of terrigenous material from free-drifting icebergs in the Weddell Sea, Deep Sea Res. Pt. II, 58, 1376–1383, 2011.

Shemesh, A., Hodell, D., Crosta, X., Kanfoush, S., Charles, C., and Guilderson, T.: Sequence of events during the last deglaciation in Southern Ocean sediments and Antarctic ice cores, Paleoceanography, 17, 8-1–8-7, 2002.

Studer, A. S., Sigman, D. M., Martínez-García, A., Benz, V., Winckler, G., Kuhn, G., Esper, O., Lamy, F., Jaccard, S. L., Wacker, L., Oleynik, S., Gersonde, R., and Haug, G. H.: Antarctic Zone nutrient conditions during the last two glacial cycles, Paleoceanography, 30, 845–862, 2015.

Stuut, J.-B. W., Crosta, X., van der Borg, K., and Schneider, R.: Relationship between Antarctic sea ice and southwest African climate during the late Quaternary, Geology, 32, 909–912, 2004.

Thomas, E. R., Allen, C. S., Etourneau, J., King, A. C. F., Severi, M., Winton, V. H. L., Mueller, J., Crosta, X., and Peck, V. L.: Antarctic Sea Ice Proxies from Marine and Ice Core Archives Suitable for Reconstructing Sea Ice over the Past 2000 Years, Geosciences, 9, 506, https://doi.org/10.3390/geosciences9120506, 2019.

Trathan, P. N., Brandon, M. A., Murphy, E. J., and Thorpe, S. E.: Transport and structure within the Antarctic Circumpolar Current to the north of South Georgia, Geophys. Res. Lett., 27, 1727–1730, 2000.

Turner, J., Hosking, J. S., Marshall, G. J., Phillips, T., and Bracegirdle, T. J.: Antarctic sea ice increase consistent with intrinsic variability of the Amundsen Sea Low, Clim. Dynam., 46, 2391–2402, 2016.

Veres, D., Bazin, L., Landais, A., Toyé Mahamadou Kele, H., Lemieux-Dudon, B., Parrenin, F., Martinerie, P., Blayo, E., Blunier, T., Capron, E., Chappellaz, J., Rasmussen, S. O., Severi, M., Svensson, A., Vinther, B., and Wolff, E. W.: The Antarctic ice core chronology (AICC2012): an optimized multi-parameter and multi-site dating approach for the last 120 thousand years, Clim. Past, 9, 1733–1748, https://doi.org/10.5194/cp-9-1733-2013, 2013.

Vernet, M., Geibert, W., Hoppema, M., Brown, P. J., Haas, C., Hellmer, H. H., Jokat, W., Jullion, L., Mazloff, M., Bakker, D. C. E., Brearley, J. A., Croot, P., Hattermann, T., Hauck, J., Hillenbrand, C. D., Hoppe, C. J. M., Huhn, O., Koch, B. P., Lechtenfeld, O. J., Meredith, M. P., Naveira Garabato, A. C., Nöthig, E. M., Peeken, I., Rutgers van der Loeff, M. M., Schmidtko, S., Schröder, M., Strass, V. H., Torres-Valdés, S., and Verdy, A.: The Weddell Gyre, Southern Ocean: Present Knowledge and Future Challenges, Rev. Geophys., 57, 623–708, 2019.

Vorrath, M.-E., Müller, J., Esper, O., Mollenhauer, G., Haas, C., Schefuß, E., and Fahl, K.: Highly branched isoprenoids for Southern Ocean sea ice reconstructions: a pilot study from the Western Antarctic Peninsula, Biogeosciences, 16, 2961–2981, https://doi.org/10.5194/bg-16-2961-2019, 2019.

Warnock, J. P., Scherer, R. P., and Konfirst, M. A.: A record of Pleistocene diatom preservation from the Amundsen Sea, West Antarctica with possible implications on silica leakage, Mar. Micropaleontol., 117, 40–46, 2015.

Weber, M. E., Clark, P. U., Kuhn, G., Timmermann, A., Sprenk, D., Gladstone, R., Zhang, X., Lohmann, G., Menviel, L., Chikamoto, M. O., Friedrich, T., and Ohlwein, C.: Millennial-scale variability in Antarctic ice-sheet discharge during the last deglaciation, Nature, 510, 134–138, 2014.

Wolff, E. W., Fischer, H., Fundel, F., Ruth, U., Twarloh, B., Littot, G. C., Mulvaney, R., Rothlisberger, R., de Angelis, M., Boutron, C. F., Hansson, M., Jonsell, U., Hutterli, M. A., Lambert, F., Kaufmann, P., Stauffer, B., Stocker, T. F., Steffensen, J. P., Bigler, M., Siggaard-Andersen, M. L., Udisti, R., Becagli, S., Castellano, E., Severi, M., Wagenbach, D., Barbante, C., Gabrielli, P., and Gaspari, V.: Southern Ocean sea-ice extent, productivity and iron flux over the past eight glacial cycles, Nature, 440, 491–496, 2006.

Wolff, E. W., Barbante, C., Becagli, S., Bigler, M., Boutron, C. F., Castellano, E., de Angelis, M., Federer, U., Fischer, H., Fundel, F., Hansson, M., Hutterli, M., Jonsell, U., Karlin, T., Kaufmann, P., Lambert, F., Littot, G. C., Mulvaney, R., Röthlisberger, R., Ruth, U., Severi, M., Siggaard-Andersen, M. L., Sime, L. C., Steffensen, J. P., Stocker, T. F., Traversi, R., Twarloh, B., Udisti, R., Wagenbach, D., and Wegner, A.: Changes in environment over the last 800 000 years from chemical analysis of the EPICA Dome C ice core, Quaternary Sci. Rev., 29, 285–295, 2010.

Wu, S., Lembke-Jene, L., Lamy, F., Arz, H. W., Nowaczyk, N., Xiao, W., Zhang, X., Hass, H. C., Titschack, J., Zheng, X., Liu, J., Dumm, L., Diekmann, B., Nurnberg, D., Tiedemann, R., and Kuhn, G.: Orbital- and millennial-scale Antarctic Circumpolar Current variability in Drake Passage over the past 140 000 years, Nat. Commun., 12, 3948, https://doi.org/10.1038/s41467-021-24264-9, 2021.

Xiao, W.: Late Quaternary climate variability in Southern Ocean Atlantic Sector, PhD, Fachbereich Geowissenschaften, Der Universitat Bremen, https://archimer.ifremer.fr/doc/00493/60451/ (last access: 6 December 2021), 2011.

Xiao, W., Esper, O., and Gersonde, R.: Last Glacial – Holocene climate variability in the Atlantic sector of the Southern Ocean, Quaternary Sci. Rev., 135, 115–137, 2016a.

Xiao, W., Frederichs, T., Gersonde, R., Kuhn, G., Esper, O., and Zhang, X.: Constraining the dating of late Quaternary marine sediment records from the Scotia Sea (Southern Ocean), Quat. Geochronol., 31, 97–118, 2016b.